Journal of Alloys and Compounds 512 (2012) 332–339

Contents lists available at SciVerse ScienceDirect

Journal of Alloys and Compounds

journal homepage: www.elsevier.com/locate/jallcom

Stress and defect induced enhanced low field magnetoresistance and dielectric constant in $La_{0.7}Sr_{0.3}MnO_3$ thin films

Sayani Majumdar[a,*], H. Huhtinen[a], H.S. Majumdar[b], P. Paturi[a]

[a] Wihuri Physical Laboratory, Department of Physics and Astronomy, University of Turku, FI-20014 Turku, Finland
[b] Department of Physics and COE for Functional Materials, Åbo Akademi University, FI-20500 Turku, Finland

ARTICLE INFO

Article history:
Received 25 May 2011
Received in revised form
28 September 2011
Accepted 30 September 2011
Available online 8 October 2011

Keywords:
Manganite
Thin films
Low-field magnetoresistance
Dielectric properties
Structural defects

ABSTRACT

Colossal magnetoresistive manganite $La_{0.7}Sr_{0.3}MnO_3$ (LSMO) films were prepared by pulsed laser deposition on three different single crystal substrates using different deposition parameters. Characterizations of their surface morphologies, structural, magnetic and magneto-transport properties show that films on MgO single crystal substrates contain higher amount of structural defects compared to those on $SrTiO_3$ (STO) and $NdGaO_3$ (NGO) substrates. Low deposition rate and thicker films give rise to polycrystallinity and grain boundaries. The films on MgO substrate showed a broad paramagnetic (PM) to ferromagnetic (FM) transition accompanied with metal–insulator transition (MIT) much below their Curie temperature (T_C) indicating growth of strained structures due to large lattice mismatch (9%) between the substrate and the film. The deposited films on STO and NGO show least effect of substrate induced strain exhibiting sharper PM–FM transition and metallic behavior below T_C. The magnetoresistance (MR) measured with 300 mT field clearly shows two contributions, one due to grain boundary tunneling and the other due to colossal MR effect. The highest low field MR effect of 17% was achieved for the film on MgO with the highest thickness and surface roughness indicating the presence of grain boundary related defects. Also a high dielectric constant was observed for the same film at room temperature up to 100 kHz frequency. Coexistence of defect induced large low-field MR and abnormally high dielectric constant can give rise to different exciting applications.

1. Introduction

Colossal magnetoresistance (CMR) in perovskite manganites has been a subject of intense research interest since late 1990s [1,2]. The family of manganites are not only interesting because of their potential applications in magnetic field sensing and memory devices but also their fascinating and intriguing physics [3,4], not completely explored so far and exciting new results are emerging constantly [5,6]. The hole-doped manganites of general composition $Re_{1-x}A_xMnO_3$ (Re = rare-earth metal, A = divalent alkali metal) shows the coexistence of different phases and depending on the composition and structural defects, these phases can be modified significantly. The transition from insulator–metal phase is generally associated with paramagnetic (PM) to ferromagnetic (FM) phase change. The FM ordering in the hole doped materials are due to mixed valence state of Mn ions, mainly in form of Mn^{3+}–O–Mn^{4+} and the interaction between them by Zener double exchange mechanism. Among different hole-doped manganites, the half-metallic manganite $La_{0.67}Sr_{0.33}MnO_3$ (LSMO) is possibly the most widely studied material as it has completely spin polarized conduction band at Fermi energy at low temperature, giving rise to 100% spin polarization. This half-metallic character has been successfully used for the spin injecting electrode in inorganic/organic spintronic devices [7,8]. Where as spintronic application requires, high quality epitaxial thin film sample with extremely smooth surface for a defect free interface between FM/non-magnetic junctions, structural defects, strains and surface roughness could also lead to interesting effects.

Due to mismatch between the film and substrate lattice parameters and oxygen non-stoichiometry in the lattice arising from improper growth conditions, the unit cell lattice is often stressed and these strained lattice structures give rise to deformed MnO_6 octahedra and thus the FM interaction and electronic conductivity is suppressed. Also the substrate induced stress causes misorientation of crystal lattice causing grain-boundary (GB) related defects. Different film growth parameters also play an important role on structural defects. One of the main defect-induced effect in polycrystalline thin-film and bulk manganite samples is the low-field magnetoresistance (LFMR) effect [9,10]. LFMR is very important for the magnetic field sensing application. LFMR has mainly been explained by the tunneling of spin polarized electrons between

* Corresponding author. Tel.: +358 2 3336240; fax: +358 2 3335070.
E-mail address: sayani.majumdar@utu.fi (S. Majumdar).

0925-8388/$ – see front matter © 2011 Elsevier B.V. All rights reserved.
doi:10.1016/j.jallcom.2011.09.093

Table 1
Sample names, their characteristic deposition parameters and approximate thicknesses.

Sample	Temperature (°C)	No. of pulses	Frequency (Hz)	Approximate thickness (nm)
S1	780	10 000	5	400
S2	780	5 000	5	200
S3	780	10 000	10	400
S4	780	15 000	10	500
S5	700	5 000	10	200

FM grains separated by GB regions. To clarify the role of these GBs, arising either from the substrate induced strain or misoriented grains due to lack of proper growth conditions, on the magnetic and electronic properties of LSMO, we have fabricated LSMO films on different substrates starting from highly lattice-mismatched MgO (∼9%) to most closely matched $SrTiO_3$ (STO) (0.87%) and $NdGaO_3$ (NGO) (−0.2%) using different pulsed laser deposition (PLD) parameters and characterized their surface morphology, structure, magnetic and transport properties thoroughly. Varying the substrates and deposition parameters, both epitaxial and less-textured films are prepared for three different thicknesses on each substrate and comparison between their different properties give the opportunity to investigate how the defect induced magnetic and transport properties evolve from highly epitaxial films to less-textured films.

2. Experimental

Preparation of stoichiometric LSMO target material for pulsed laser deposition (PLD) was reported earlier [11]. Phase purities of the PLD targets were checked by X-ray diffraction (XRD) using Cu Kα radiation. LSMO films were grown on the MgO (1 0 0), STO (1 0 0) and NGO (1 0 0) polished single crystal substrates at temperatures (T_S) of 700 °C and 780 °C using the laser repetition rates of 5 Hz and 10 Hz and the pulse energy of 2 J/cm^2. The target to substrate distance was 35 mm and oxygen pressure in the deposition chamber was 0.25 Torr. These two parameters were chosen by observing the optimum plume formation and were kept constant for all the films. Films with different thicknesses were obtained by using 5 000, 10 000 and 15 000 pulses and the approximate thicknesses are 200, 400 and 500 nm, respectively. On each substrate, five LSMO films, deposited by different deposition parameters, were grown, as listed in Table 1.

After deposition, the films were subjected to post-annealing treatments in 1 atm pressure of oxygen for 10 min at the deposition temperature and then cooled to room temperature at the cooling rate of 20 °C/min. The surface morphologies of the films were characterized by atomic force microscopy (AFM) in non-contact mode and their compositions and lattice structures were investigated by X-ray diffraction (XRD) using a Bragg–Brentano diffractometer (Model Philips PW3710). The magnetic properties were investigated with a SQUID magnetometer in the range of 5–400 K. The resistivities were measured using the four probe method in the range 5–300 K in the absence and presence of a magnetic field of B = 300 mT and LFMR were measured by sweeping the in-plane magnetic field between −300 and +300 mT and back at a fixed temperature. The impedance spectra were measured at room temperature with a Gamry 600^{TM} Potentiostat in a frequency range of 1 Hz to 1 MHz. The amplitude of the AC bias was 20 mV rms. The DC bias was varied from 0 to 1 V.

3. Results and discussion

3.1. Surface morphology

Fig. 1 shows the surface structures of the LSMO films deposited on different substrates. Although the surface features of the films were initially identified as almost similar [11], more detail inspection reveals that films grown on MgO have bigger domains compared to the surface structures of the films grown on STO and NGO. Also, the domains are more closely packed in the films on STO and NGO compared to that on MgO, where the domains have more island type growth. These features remain unchanged when the films were prepared by varying the frequency of the PLD pulses and T_S. However, the rms roughnesses of the films differ significantly due to variation in both the PLD pulse frequency and T_S.

Surface rms roughness values for as-grown films are calculated as an average from AFM images taken from different 5 μm × 5 μm areas of the films and the standard deviation in rms roughness value is ±1.2 nm, 1.0 nm and 0.4 nm for MgO, STO and NGO, respectively. The roughness increases with thickness in all substrates. Lower deposition temperature leads to the smoothest surface for all the substrates, especially on STO. For films on MgO, STO and NGO, the rms roughness is 9 nm, 3.7 nm and 9.1 nm, respectively, for T_S = 700 °C. However, the roughness value increases appreciably reaching 18.6 nm, 15 nm and 14.4 nm, respectively, for T_S = 780 °C. In addition, the higher deposition frequency (10 Hz) also leads to the smoother surface especially for films on STO and NGO. This leads to the conclusions that lower laser frequency, higher deposition temperature and increasing film thickness lead to more structural defects in the films. This could be explained with the difference in growth mechanisms affected by the different deposition parameters as well as the lattice mismatch between the film and the substrate [12,13].

3.2. Structural analysis

The room temperature XRD measurements show that the crystalline structure of the LSMO target is rhombohedral perovskite with space group $R\bar{3}C$ and lattice parameters a_h = 0.5473 nm and

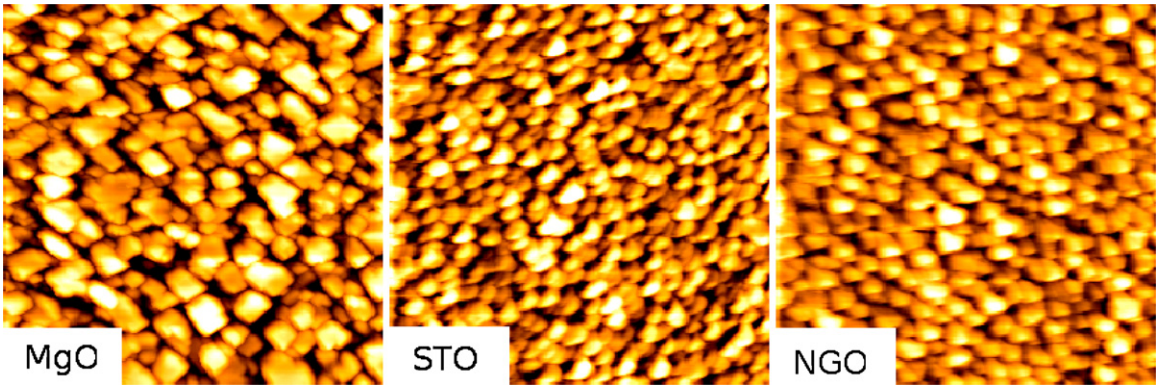

Fig. 1. AFM images (5 μm × 5 μm) of the LSMO films deposited on MgO, STO and NGO substrates with T_S = 780 °C, 10 000 laser pulses with frequency of 10 Hz. The grey scale (height from black to white) is 70 nm for all the films on MgO, STO and NGO.

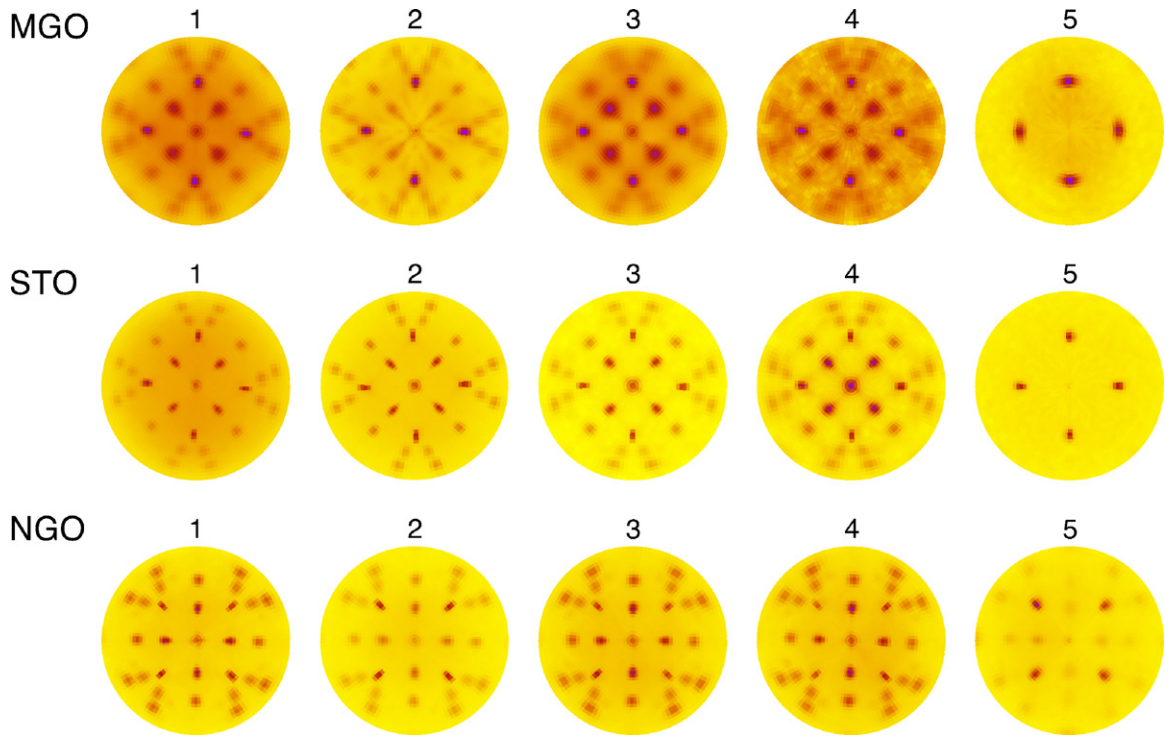

Fig. 2. X-ray pole figures of the (1 1 0) reflection at $2\theta = 32.76^\circ$ of as deposited LSMO films S1–S5 on MgO, STO and NGO substrates using deposition parameters shown in Table 1.

$c_h = 1.336$ nm (pseudo-cubic $a_c = 0.3866$ nm). More detailed structural analysis of these films is reported earlier [11]. The films grown on MgO, STO and NGO substrates, depending on the deposition parameters show either complete epitaxial growth, i.e. LSMO pseudo-cubic structure with diffraction peaks matching with the substrate peaks, or a less textured growth with a mixture of (1 0 0), (1 1 0) and (1 1 1) peaks.

The X-ray pole figures (φ–ψ scans) of the (1 1 0) reflection at $2\theta = 32.76^\circ$ (Fig. 2) show several crystalline orientations in most of the samples. Only the samples S5 on MgO and STO are fully and on NGO are nearly textured with (1 0 0) perpendicular to the plane of the film. All the other films have additional orientations with pseudocubic axis in 10°, 13°, 16° and 27° angles with the substrate (0 0 1) axis. There are also several in-plane directions. In addition, the samples on MgO have much wider peaks than the samples on STO or NGO, indicating low angle grain boundaries within a single grain orientation. The pole figures unambiguously show that samples S1–S4 on all the substrates contain large amount of low and high angle grain boundaries, especially the sample S4 on MgO.

3.3. Magnetic properties

Fig. 3(a) shows the field cooled (FC) magnetization measurements on the LSMO/MgO films with in-plane external magnetic field $B = 10$ mT and the inset of Fig. 3(a) shows the FC magnetization of the LSMO target in the field of $B = 8$ mT. Curie temperature (T_C) of 347.8 K was obtained from the target. For LSMO/MgO films, T_C value changes substantially depending on the deposition parameters. Although the onset of PM–FM transition is close to that of the target material, in all the cases, except for sample S5, the nature of transition is broad and saturation magnetic moment (M_S) value was not reached until 5 K which may be associated with the influence of a distribution of magnetic domains in the films. Some of the domains contain higher strain related defects and distorted MnO_6 octahedra resulting in reduced T_C while the domains containing lesser defects show T_C close to the target material. Average magnetic moment from the whole film gives rise to a smooth and broad magnetic transition. Considering the higher lattice mismatch (~9%) between MgO and LSMO, it is justified to assume that the layers closest to the substrate are the most strained ones and hence contain substantial amount of defects. With increasing thickness, less strained LSMO with higher T_C starts to grow. This hypothesis is supported by the fact that the two thinnest films on MgO have the lowest T_C (~330 K). The coercive fields (H_C) of the films are high (~26 mT at 5 K) and the transition is broad (Fig. 3(b)) except for the film S5, with better crystalline properties, where H_C is 14 mT at 5 K and also the PM–FM transition is much sharper. This clearly indicates that structural distortions in these films cause strong pinning centers for the magnetic domain movement increasing the coercivity. No measurable differences between ZFC and FC branches were detected in any samples showing complete FM ordering for all samples.

For the films on STO and NGO, T_C does not depend strongly on the deposition parameters and thicknesses, though the thinnest film S5 on STO has T_C of 342 K, approximately 10 K lesser than the other films. From the calculation of in-plane lattice parameters, S5 shows the highest compressive strain among the films on STO [11] and so we can conclude that at lower temperatures the LSMO grows with elongated c-axis and that this structural disorder results in lower T_C. Also this film shows a broad magnetic transition like the LSMO/MgO films showing the influence of strained lattices on the magnetic properties. However, all the other films on STO have very sharp PM to FM transition and M_S value is reached approximately at 250 K (Fig. 4(a)). H_C is smaller than the films on MgO and varies between 17 mT and 20 mT at 5 K and between 12 mT and 4 mT at 100 K for different growth conditions (Fig. 4(b)).

Films on NGO show a high paramagnetic signal from the substrate at low temperatures making it difficult to distinguish between the contributions of the film and the substrate at 5 K. However, the T_C values are measured accurately from the high temperature scans showing that these films have the highest T_C, even higher than that of the target material (Fig. 5(a)). The two

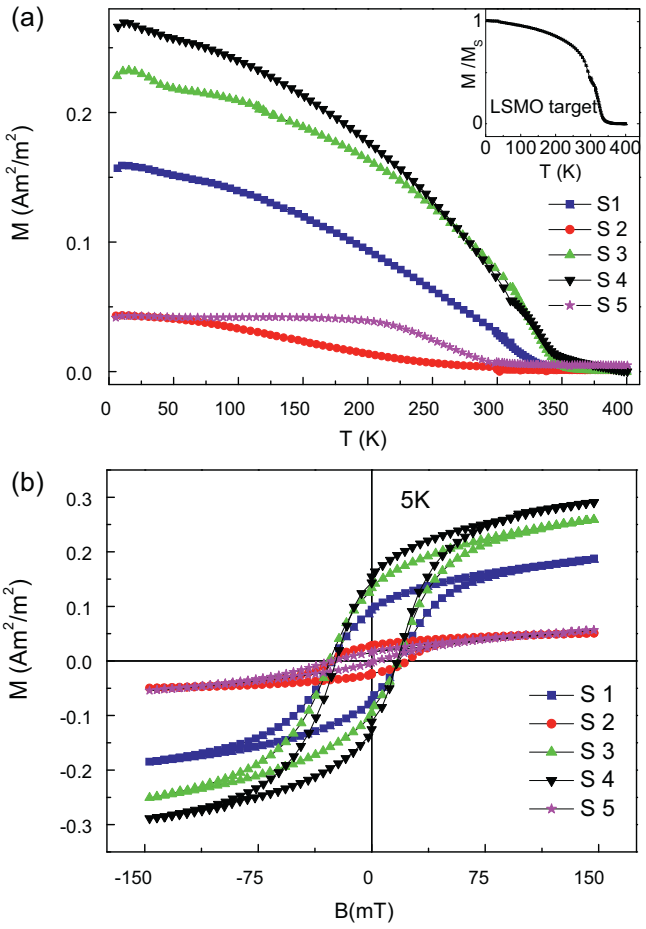

Fig. 3. (a) Temperature dependence of field-cooled (FC) magnetization of the LSMO/MgO films per unit area and the target per unit mass (inset) and (b) hysteresis loop measurement at 5 K for the same films.

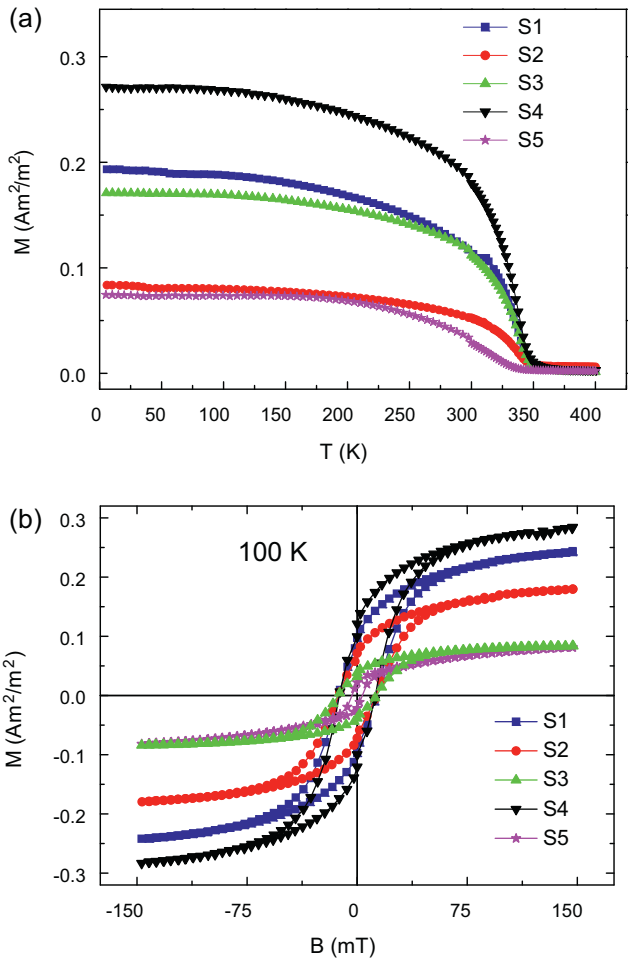

Fig. 4. (a) Temperature dependence of FC magnetization of the LSMO/STO films per unit area and (b) hysteresis loop measurement at 100 K for the same films.

thinnest films S2 and S5 show better crystalline growth and the highest values of T_C confirming that they have minimal amount of strains and related defects and are hence very suitable for spin injection purposes. H_C at 100 K (Fig. 5(b)) are between 14 mT and 4 mT for different samples, matching closely with the H_C values for the LSMO/STO films and the transition is also very sharp.

3.4. Resistivity and magnetoresistance

Fig. 6(a) shows sheet resistance (R) per unit area as a function of temperature for all the deposited films on MgO in the absence and presence of magnetic fields (B) of 300 mT. Depending on the deposition parameters, the resistance changes by orders of magnitude. The highest resistivity was obtained for the thickest film S4. All the films show metal–insulator transition (MIT) much below their respective T_Cs suggesting the presence of GB effects in these films. Also the calculated value of MR, defined as $(R(0) - R(B))/R(0)$, as a function of temperature is plotted in Fig. 6(b) and it shows a distinct maximum in MR around MIT temperature (T_{MIT}) for all the samples except S5.

Fig. 6(c) shows resistance hysteresis loops for all the films deposited on MgO substrate. The LFMR observed from the resistance hysteresis loops at low temperatures with the appearance of two peaks close to H_C support the presence of GB tunneling MR in all the films [9]. The LFMR value, calculated by taking the highest R value as R_{AP} and lowest R value as R_P and putting them in the formula $(R_{AP} - R_P)/R_P$, is the largest (17.5%) for the film S4, having the largest resistance and lowest T_{MIT}. For all the other samples, the LFMR vary between 5 and 7%. This suggests that, above certain thickness, the films on MgO show deteriorated crystalline properties and higher GBs. Charge carriers suffer scattering at the GBs decreasing the conductivity of the sample. The MR in the LSMO films with low fields can be understood in terms of the tunneling of spin polarized conduction electrons at the boundaries between FM grains. Upon application of a magnetic field, resistance starts changing showing a resistivity maximum at the H_C and decrease as the relative orientation of the magnetic moment between the FM grains changes with the application of a magnetic field. The MR curves are closely correlated with the magnetic hysteresis loops. The maxima in the resistance occur at the magnetic coercive field when the magnetization, M, equals zero and the rotation towards a complete alignment of moments cause a reduction of the resistance. LFMR is the highest at 5 K and decreases with increasing temperature. So clearly, the MR responses of these films have two components, one due to LFMR arising from GB defects and the other due to CMR property of the bulk LSMO.

For the films grown on STO and NGO (Figs. 7 and 8(a), respectively), all the samples have metallic resistivity in the temperature range of 5–300 K and T_{MIT} is higher than 300 K, very close to T_C, showing much less GB and stress related defects in them. Samples S1, S2 and S5 show higher sheet resistance at 300 K for the films on STO while S3 on NGO has the maximum resistance at 300 K. % MR as a function of temperature is also plotted in Figs. 7 and 8(b) and it shows a peak at low temperature followed by a decrease in MR values until 250 K. Above 250 K, MR again starts to increase,

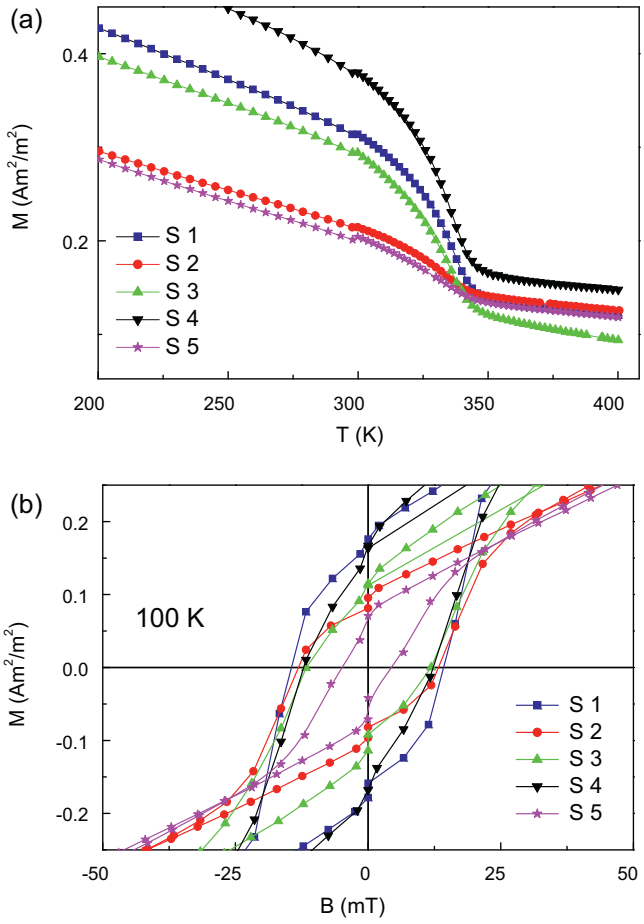

Fig. 5. (a) Temperature dependence of FC magnetization of the LSMO/NGO films per unit area and (b) hysteresis loop measurement at 100 K for the same films.

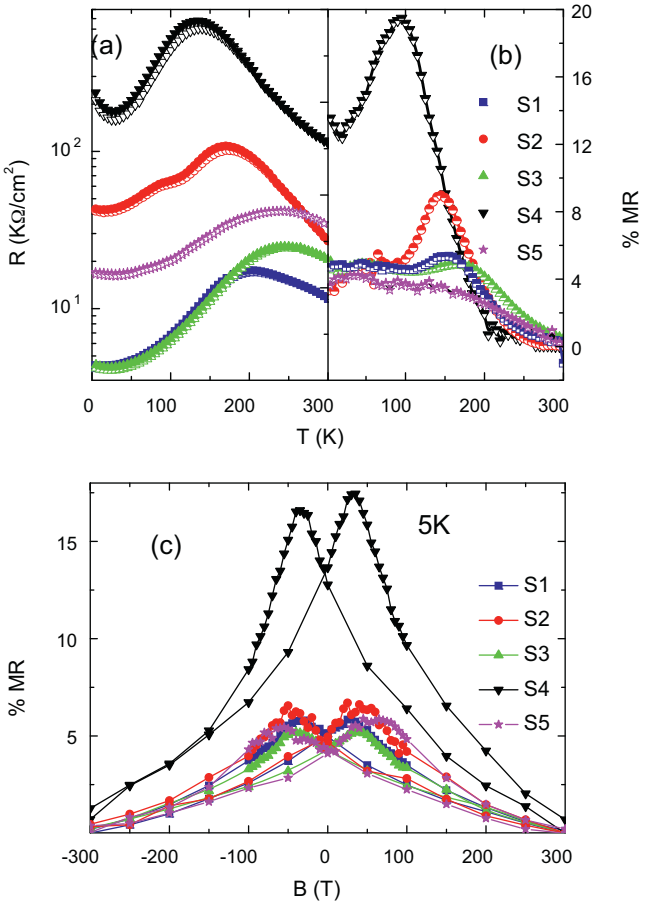

Fig. 6. (a) Resistance per unit area with and without a magnetic field (B) of 300 mT, solid symbols are R in absence of B, open symbols are R in presence of B = 300 mT. (b) % MR of LSMO/MgO films as a function of temperature and (c) resistance hysteresis at 5 K for the same films.

possibly for a second maximum around T_{MIT}. For S5 on STO, the MR peak around T_{MIT} is observed at 270 K, indicating that T_{MIT} for this film is close to room temperature, which is expected considering the lowest T_C in this film. The LFMR effect (Figs. 7 and 8(c)), characteristics of the GB tunneling, is much smaller, close to 1–3%, in films on STO and NGO again confirming lesser structural defects in these films. The lowest LFMR on STO substrate is observed for sample S2 and S5, having thickness close to 200 nm. However, S5 on NGO shows lowest LFMR effect (0.6%) among all the samples and hence the smallest amounts of GBs are expected in this film.

For the in-depth analysis of the transport properties induced by defects, two samples S3 and S4 on MgO having 5% and 17% LFMR were chosen. Fig. 9(a) and (b) shows the plot of LFMR, magnetization and MR of S3 and S4, respectively, as a function of temperature. Clearly, the trend is similar in every case for S3, i.e., low temperature saturation below 150 K followed by a sharp decrease. However, LFMR response of S4 is distinctly different from that of S3. In S4, LFMR starts to increase sharply below 100 K, compared to the low temperature saturation in S3 (shown by the dotted line for a guide to the eye). This indicates additional electron lattice scattering at the GBs in S4, which reduces considerably under application of external magnetic fields, producing large MR effects. The MR peak around T_{MIT} is observed for both S3 and S4, as discussed earlier. LFMR starts decreasing faster than the bulk magnetization for both S3 and S4. This is expected considering the fact that LFMR was measured on the LSMO film surface where due to breaking of the bonds of MnO_6 octahedra, spin polarization starts to decrease much faster than the bulk film [14].

The dependence of MR on spin-polarized tunneling has earlier been described by Helman and Abelest [15]. They showed that MR could be approximately described as MR $\sim -A(M/M_S)^2$, where the prefactor A determines the magnitude of MR and depends on the number and the size of FM particles. To examine the mechanism of the LFMR effect in S3 and S4, we fitted the MR data of the samples at different temperatures to the $(M/M_S)^2$ dependence. Fig. 10 shows the fitting for S3 at 5 K and for S4 at 5 and 100 K. We observed excellent fittings for S3 at 5 K, where as, the fitting is not very nice for S4, especially at 5 K. At 100 K, the fitting for S4 is clearly better. These results, therefore, confirm that the main mechanism for the LFMR effect in S3 is the spin-polarized-tunneling effect at the boundaries between FM grains. In S4, the resistance maxima shift towards higher magnetic field side below 100 K, which clearly indicates that due to increased electron-lattice scattering in S4, a larger magnetic field is needed to suppress the scattering. Also there is a possibility of trapped electrons in this sample due to increased defects and these trapped charges at lower temperature under magnetic field form bound magnetic polarons which act as localized FM clusters. These localized clusters can switch at different fields and tunneling between FM grains can be modified. With increasing temperature, reduced LFMR implies that the electron-scattering mechanism at the GBs become dominant due to a narrowing of the FM grain size and reducing spin polarization of the carriers. Above 150 K, a drastic decrease in LFMR is a direct consequence of decreasing FM grain size near T_C.

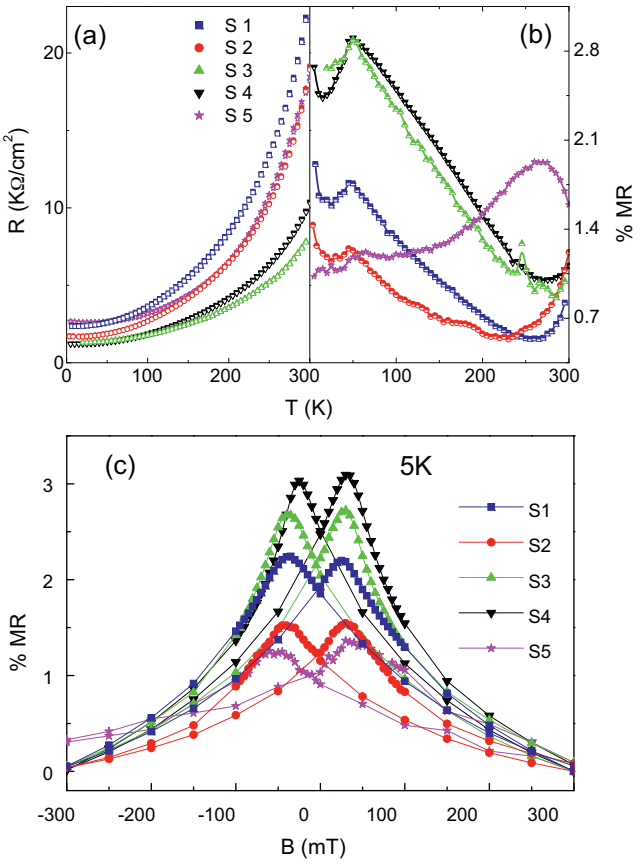

Fig. 7. (a) Resistance per unit area with and without B of 300 mT, solid symbols are R in absence of B, open symbols are R in presence of B = 300 mT. (b) % MR of the LSMO/STO films as a function of temperature and (c) resistance hysteresis at 5 K for the same films.

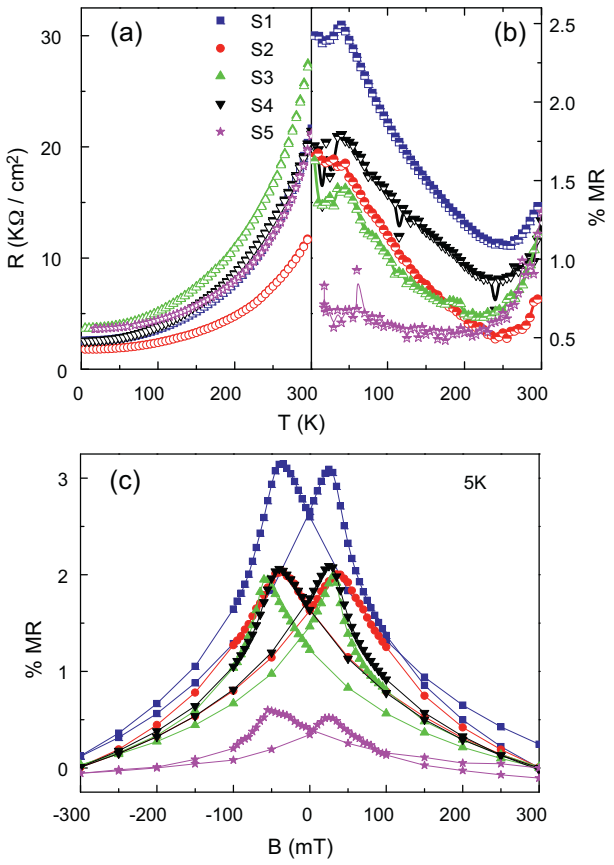

Fig. 8. (a) Resistance per unit area with and without B of 300 mT, solid symbols are R in absence of B, open symbols are R in presence of B = 300 mT. (b) % MR of the NGO films as a function of temperature and (c) resistance hysteresis at 5 K for the same films.

3.5. Impedance spectroscopy

For an insight of the microscopic nature of the GB region, a complex impedance spectroscopy measurement is performed on samples S3 and S4 on MGO at room temperature in the frequency range 1 Hz to 1 MHz. Fig. 11(a) shows the real and imaginary impedance (Z' and Z'', respectively) as a function of frequency for S3 and S4. Z' is frequency independent below 10 kHz for S3 where as Z' of S4 starts to decrease even below 1 kHz showing the existence of stronger capacitive effect in S4 compared to S3. This is expected considering higher GB defects in S4. The negative value of imaginary impedance Z'' shows a maximum at 40 kHz for S3 and 2.5 kHz for S4. This frequency, where Z'' shows a maximum, ω_{max}, is related to the dielectric relaxation of the sample [16]. Smaller ω_{max} in S4 indicates higher dielectric relaxation time in S4 compared to S3 and is a direct consequence of higher capacitance due to GB effect. The obtained Z'' for both the samples were fitted using equivalent circuits consisting of three RC circuits which signifies that there are different contributions of grains and GB resistive (R) and capacitive (C) components.

The dielectric constant, ε' of S3 and S4 as a function of frequency is plotted in Fig. 11(b). An abnormally high value of ε' of S4 (60 000) at lower frequencies is obtained which is comparable to the colossal dielectric constant (CDC) values of 10^3 to 10^5 reported in CDC compounds [17]. The ε' starts to decrease drastically above 10 kHz reaching the permittivity of the order of 10^2 at 1 MHz. ε' of S3 at lower frequencies is much less than that of S4 (15 000) but remains constant almost until 100 kHz and a higher permittivity at 1 MHz frequency. Hence, it becomes obvious that GB effect in S4 plays a major role to enhance ε' at lower frequencies. The grains and GBs possess different conductivity and capacitance which leads to Maxwell–Wagner-type polarization and a Schottky barrier at the interface. These interface depletion layers contribute to large dielectric dispersion as higher frequencies are approached [18].

The dielectric loss factor, tan δ, calculated from the experimental data at 300 K, measured with different bias voltages as a function of frequency is shown in Fig. 12. The applied dc voltages were 0, 0.1, 0.25, 0.5, 0.75 and 1 V and the arrow indicates the direction of increasing voltage. The plot shows decrease in dielectric loss in S4 from ~38 at 100 Hz to a minimum of ~1 at 10 kHz. In S3, tan δ is much higher ~280 at 200 Hz and decreases to ~2 at 10 kHz. Application of dc bias increases loss tangent shifting the minimum to the higher frequency side for both S3 and S4, similar to the temperature dependence of tan δ [17].

The Nyquist diagram or a Cole–Cole plot of the impedance data (not shown here) for S3 and S4 shows a semicircle with non-zero intercept. It is known that one semicircle in the plot is associated with the intrinsic property of the material whereas two or more successive or overlapped or distorted semicircles are associated with the excess contribution of the GB and/or electrodes [19]. In the present case, the fitting of S3 and S4 distinctly shows an overlapping of three semicircles indicating three equivalent RC circuits needed to explain the data. So, the observed effect is mainly extrinsic in nature and GB related defects in the film play a major role in exhibiting CDC values.

With increasing bias, the impedance of both S3 and S4 decreases significantly. With increasing bias voltage, the decrease in

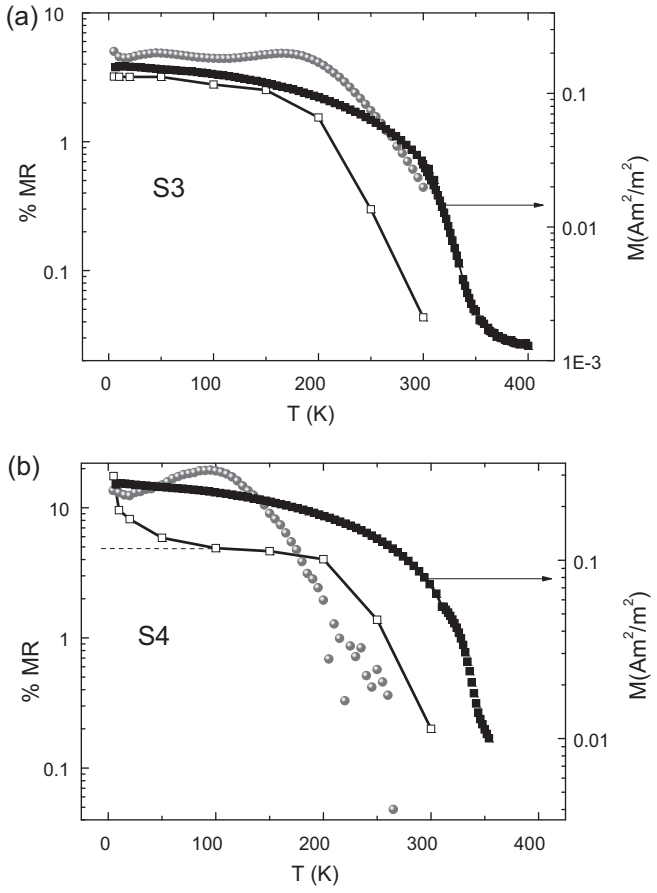

Fig. 9. % MR (grey circles), LFMR (open squares) and magnetization (solid squares) as a function of temperature for sample (a) S3 and (b) S4.

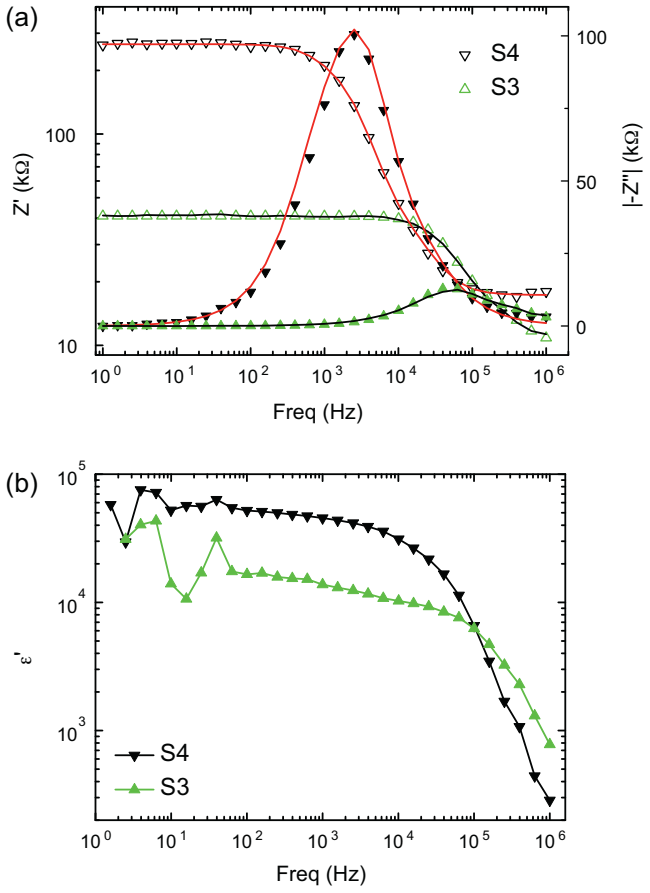

Fig. 11. (a) Real and imaginary impedance (open and solid circles, respectively) as a function of frequency for sample S3 (black) and S4 (red circles) at 300 K. Solid line is a fit of experimental data with three equivalent *RC* circuits. (b) Dielectric constant ε' of S3 and S4 as a function of frequency at 300 K. (For interpretation of the references to color in this figure legend, the reader is referred to the web version of the article.)

resistance was also observed earlier by Rao [20] and Parashar et al. [21] and was attributed to electric field-induced magnetization in manganites and close correlation between magnetic and electric order parameters. In the present case, the change in resistance with bias is more significant than change in capacitance and the possibility of electric field induced ferromagnetism can not be ruled out. The temperature and magnetic field dependent study

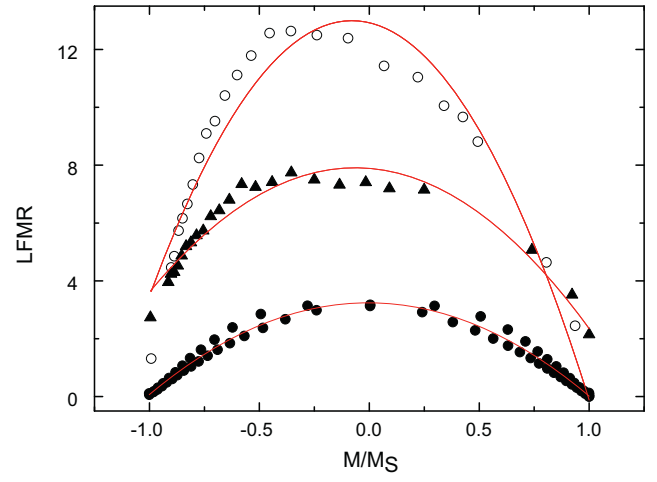

Fig. 10. LFMR as a function of magnetization ratio (M/M_S) for sample S3 at 5 K (solid circles) and S4 at 5 K (open circles) and 100 K (solid triangles). Red line is a fit of polynomial of second order. (For interpretation of the references to color in this figure legend, the reader is referred to the web version of the article.)

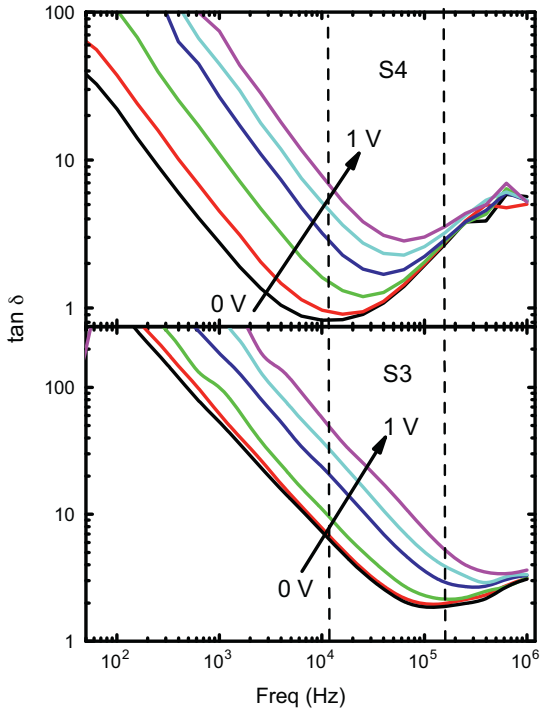

Fig. 12. Loss tangent ($\tan\delta$) as a function of frequency for sample S3 (lower panel) and S4 (upper panel) measured with different bias voltages.

of complex impedance spectroscopy is underway to clarify this issue.

So through the structural, magnetic and transport studies of the LSMO films on different substrates it is shown that films with higher structural and grain boundary related defects can give rise to high LFMR and higher dielectric constants and could lead to a novel route for defect induced multiferroic properties in manganites.

4. Conclusions

To conclude, we have prepared LSMO films by pulsed laser deposition on three different single crystal substrates with the lowest lattice mismatched $SrTiO_3$ and $NdGaO_3$ to completely mismatched MgO varying different PLD parameters and thickness and studied their surface morphology, structural, magnetic and transport properties in detail. Lower film growth rate and higher film thickness give rise to polycrystallinity and grain boundaries, especially on MgO. With increasing defect and GB concentration, the low field MR and dielectric constant of the film increases significantly. Interplay between this magnetic and electric field coupling through the introduction of defects can lead to interesting new preparation route for different materials attractive for low field sensor and other applications.

Acknowledgement

Financial support from Jenni and Antti Wihuri Foundation, Turku Collegium for Science and Medicine and Academy of Finland is acknowledged.

References

[1] R. Mahesh, R. Mahendiran, A.K. Raychaudhuri, C.N.R. Rao, J. Solid State Chem. 120 (1995) 204–207.
[2] P.G. Radaelli, G. Iannone, M. Marezio, H.Y. Hwang, S.-W. Cheong, J.D. Jorgensen, D.N. Argyriou, Phys. Rev. B 56 (1997) 8265–8276.
[3] A. Dagotto, T. Hotta, A. Moreo, Phys. Reports 344 (2001) 1–153.
[4] C.N.R. Rao, A.K. Raychaudhuri, Colossal magnetoresistance, charge ordering and other novel properties of manganates and other related materials, in: C.N.R. Rao, B. Raveau (Eds.), Colossal Magnetoresistance, Charge ordering and Related Properties of Manganese Oxides, World Scientific, Singapore, 1998, pp. 1–42.
[5] R. Mohan, N. Kumar, B. Singh, N.K. Gaur, S. Bhattacharya, S. Rayaprol, A. Dogra, S.K. Gupta, S.J. Kim, R.K. Singh, J. Alloys Compd. 508 (2010) 32–35.
[6] J. Hu, Y. Wang, Y. Zhang, H. Liu, H. Qin, B. Li, J. Alloys Compd. 509 (2011) 1360–1363.
[7] M. Bowen, M. Bibes, A. Barthélémy, J.-P. Contour, A. Anane, Y. Lemaître, A. Fert, Appl. Phys. Lett. 82 (2003) 233–235.
[8] Z.H. Xiong, D. Wu, Z. Valy Vardeny, J. Shi, Nature 427 (2004) 821–824.
[9] A. Gupta, G.Q. Gong, G. Xiao, P.R. Duncombe, P. Lecoeur, P. Trouilloud, Y.Y. Wang, V.P. Dravid, J.Z. Sun, Phys. Rev. B 54 (1996) R15629–R15632.
[10] N.D. Mathur, G. Burnell, S.P. Isaac, T.J. Jackson, B.-S. Teo, J.L. MacManus-Driscoll, L.F. Cohen, J.E. Evetts, M.G. Blamire, Nature 387 (1997) 266–268.
[11] S. Majumdar, H. Huhtinen, H.S. Majumdar, R. Laiho, R. Österbacka, J. Appl. Phys. 104 (2008), 033910-1–033910-6.
[12] T. Frey, C.C. Chi, C.C. Tsuei, T. Shaw, F. Bozso, Phys. Rev. B 49 (1994) 3483–3491.
[13] G. Koster, G.J.H.M. Rijnders, D.H.A. Blank, H. Rogalla, Appl. Phys. Lett. 74 (1999) 3729–3731.
[14] V. Garcia, M. Bibes, A. Barthélémy, M. Bowen, E. Jacquet, J.-P. Contour, A. Fert, Phys. Rev. B 69 (2004) 052403–052406.
[15] J.S. Helman, B. Abelest, Phys. Rev. Lett. 37 (1976) 1429–1432.
[16] D.P. Almond, A.R. West, Solid State Ionics 11 (1983) 57–64.
[17] A. Podpirka, S. Ramanathan, J. Appl. Phys. 109 (2011), 014106-1–014106-7.
[18] P. Lunkenheimer, V. Bobnar, A.V. Pronin, A.I. Ritus, A.A. Volkov, A. Loidl, Phys. Rev. B 66 (2002) 052105–052108.
[19] J.H. Lee, H. Chou, G.H. Wen, G.H. Hwang, J. Appl. Phys. 107 (2010), 023907-1–023907-4.
[20] C.N.R. Rao, J. Phys. Chem. B 104 (2000) 5877–5889.
[21] S. Parashar, L. Sudheendra, A.R. Raju, C.N.R. Rao, J. Appl. Phys. 95 (2004) 2181–2183.